SIAM J. APPL. MATH.
Vol. 73, No. 6, pp. 2124–2142

A MODIFIED OSTER–MURRAY–HARRIS MECHANICAL MODEL OF MORPHOGENESIS*

BENJAMIN L. VAUGHAN, JR.†, RUTH E. BAKER‡, DAVID KAY§, AND PHILIP K. MAINI‡

Abstract. There are two main modeling paradigms for biological pattern formation in developmental biology: chemical prepattern models and cell aggregation models. This paper focuses on an example of a cell aggregation model, the mechanical model developed by Oster, Murray, and Harris [*Development*, 78 (1983), pp. 83–125]. We revisit the Oster–Murray–Harris model and find that, due to the infinitesimal displacement assumption made in the original version of this model, there is a restriction on the types of boundary conditions that can be prescribed. We derive a modified form of the model which relaxes the infinitesimal displacement assumption. We analyze the dynamics of this model using linear and multiscale nonlinear analysis and show that it has the same linear behavior as the original Oster–Murray–Harris model. Nonlinear analysis, however, predicts that the modified model will allow for a wider range of parameters where the solution evolves to a bounded steady state. The results from both analyses are verified through numerical simulations of the full nonlinear model in one and two dimensions. The increased range of boundary conditions that are well-posed, as well as a wider range of parameters that yield bounded steady states, renders the modified model more applicable to, and more robust for, comparisons with experiments.

Key words. pattern formation, mechanochemical models, morphogenesis, multiscale analysis

AMS subject classification. 92

DOI. 10.1137/120891733

1. Introduction.

Most models of morphogenesis are prepatterning models; they assume that a spatially varying chemical prepattern is set up to which cells respond in a concentration-dependent manner. The simplest such model is the gradient model, first proposed by Wolpert in 1969 [32], where a source-sink arrangement establishes a gradient of chemical morphogen. A more complex model is the Turing reaction-diffusion model [31], in which a system of chemicals, reacting and diffusing, are driven unstable by diffusion and evolve into spatially heterogenesis patterns of varying complexity, depending on the domain size, geometry, and imposed boundary conditions.

In the above modeling framework, the initial cell density is spatially uniform, but the cells respond to the chemical in a spatially nonuniform manner due to the spatially varying chemical concentration. An alternative modeling paradigm is one in which the cells themselves form a spatially nonuniform pattern and then differentiate in a density-dependent manner. Such patterns in cell density can arise in a number of ways. For example, the cells may secrete a chemical (termed a chemoattractant) and move up gradients in that chemical. This leads to a coupled system of reaction-diffusion

*Received by the editors September 17, 2012; accepted for publication (in revised form) August 15, 2013; published electronically November 21, 2013.
http://www.siam.org/journals/siap/73-6/89173.html

†Centre for Mathematical Biology, Mathematical Institute, University of Oxford, Oxford OX1 3LB, UK, and Department of Mathematical Sciences, University of Cincinnati, Cincinnati, OH 45221 (vaughabn@ucmail.uc.edu). This author's work was partially supported by St. John's College, Oxford.

‡Centre for Mathematical Biology, Mathematical Institute, University of Oxford, Oxford OX1 3LB, UK (ruth.baker@maths.ox.ac.uk, maini@maths.ox.ac.uk). The fourth author's work was partially supported by a Royal Society Wolfson Research Merit Award.

§Department of Computer Science, University of Oxford, Oxford OX1 3QD, UK (dkay@cs.ox.ac.uk).

type with a nonlinear advection term, which can yield spatial patterns in cell density and chemical concentration. A completely different modeling framework, from both biological and mathematical perspectives, is the mechanical (or mechanochemical) framework. Here, it is proposed that the mechanical interactions between cells and the extracellular matrix in which they reside lead to physical cues to which cells respond. Chemical signaling can be incorporated as necessary. The resultant system of equations is of mixed parabolic-hyperbolic-elliptic type and has been shown to exhibit spatial patterning in cell density.

While both of these modeling frameworks have been used to describe pattern formation, due to its very complex mathematical form, the mechanical models have been studied in much less mathematical and numerical depth than the chemical reaction-diffusion and chemotactic models. In this paper, we focus on the mechanical modeling approach. For a detailed discussion of the differences between chemical prepatterning and mechanical models, we refer the reader to [17].

The role of mechanical forces in morphogenesis was explored by Odell et al. [24], and the Oster–Murray–Harris model, hereafter referred to as OMH, was introduced by Oster, Murray, and Harris [21, 26]. This model considers the role of mechanical forces in pattern formation during morphogenesis and, as such, does not separate the patterning process from the mechanical mechanisms for forming patterns and shape. It has been studied in various forms by numerous authors analytically and numerically as well as experimentally [1, 2, 3, 4, 5, 6, 7, 9, 11, 14, 15, 16, 18, 19, 20, 22, 23, 25, 27, 29, 30]. For a detailed overview of the OMH model, see [17].

Linear analysis shows that both the Turing-type models and the mechanical models can be driven linearly unstable and evolve to spatially structured steady state patterns. To date, application of the mechanical model to problems in pattern formation have used mainly simple periodic boundary conditions. To extend the application of these mechanical models to a wider range of experimental protocols, such as fibroblast-populated collagen lattice (FPCL) assays [8] and fibroblast-populated collagen microsphere (FPCM) assays [16, 30], requires alternative boundary conditions which are not consistent with the simplifications made in the derivation of the original OMH model.

We have presented a modified version of the original OMH model in Gilmore et al. [10] and illustrated its use for periodic boundary conditions on a one-dimensional domain. In this paper, we significantly extend the application of the modified model by showing that a larger range of boundary conditions can be imposed. To our surprise, we find that this modified model exhibits bounded steady state solutions for a wider range of parameter values, which improves the model's robustness when making comparisons with experiments. We analyze the updated model using linear and multiscale nonlinear analysis. Additionally, numerical simulations of the full nonlinear equations are performed in both one and two dimensions to verify the results of the analysis. The paper is organized as follows. We reintroduce the OMH model in section 2 and discuss its limitations concerning the range of well-posed boundary conditions. In section 3, we derive a modified version of the OMH model that allows a wider range of well-posed boundary conditions. We perform linear analysis on the updated model for small perturbations of the uniform steady state in section 4 and multiscale nonlinear analysis near a bifurcation point in section 5. The results of numerical simulations of the full system of nonlinear equations in one dimension are given in section 6, and results in two dimensions are given in section 7. Section 8 contains a summary of results and conclusions.

2. Oster–Murray–Harris mechanical model. The OMH model of mesenchymal morphogenesis [21, 26] is based on two properties of mesenchymal cells: that mesenchymal cells migrate within a substratum consisting of a fibrous extracellular matrix (ECM) and that these motile cells can exert large traction forces on the ECM. For simplicity, we neglect active cell motion in their model and assume that the only motion of the cells is due to displacement of the ECM medium. From conservation of mass, the equation governing the evolution of the cell density is

$$\frac{\partial c}{\partial t} + \nabla \cdot \left(c \frac{\partial \boldsymbol{u}}{\partial t} \right) = 0, \tag{2.1}$$

where c is the cell density and $\boldsymbol{u}$ is the vector representing the displacement of the ECM. The ECM is modeled as a linear viscoelastic medium, and the resulting force balance equation governing the displacement of the ECM is

$$\nabla \cdot \left(\boldsymbol{\sigma} + \tau \phi \left(c, \rho \right) \mathbf{I} \right) = \rho \boldsymbol{B}, \tag{2.2}$$

where $\boldsymbol{\sigma}$ is the stress tensor, $\tau \phi \left(c, \rho \right)$ is the traction force exerted by the cells, $\mathbf{I}$ is the identity tensor, ρ is the ECM density, and $\boldsymbol{B}$ represents the body forces. It is assumed that the body force is Hookean, hence $\boldsymbol{B} = s\boldsymbol{u}$, where s is a spring constant that measures the strength of the restoring force. Since the ECM is modeled as a linear viscoelastic medium, the stress tensor is

$$\boldsymbol{\sigma} = \underbrace{\mu_1 \frac{\partial \boldsymbol{e}}{\partial t} + \mu_2 \frac{\partial \theta}{\partial t} \mathbf{I}}_{\text{viscous damping forces}} + \underbrace{E \left(\boldsymbol{e} + \nu' \theta \mathbf{I} \right)}_{\text{elastic forces}}, \tag{2.3}$$

where μ_1 and μ_2 are the shear and bulk viscosities, respectively, $\boldsymbol{e} = \left(\nabla \boldsymbol{u} + \nabla \boldsymbol{u}^T \right) / 2$ is the linear strain tensor, $\theta = \nabla \cdot \boldsymbol{u}$ is the dilation, E is the Young's modulus, and $\nu' = \nu / \left(1 - 2\nu \right)$, where ν is the Poisson ratio [13]. The traction force is modeled using the function

$$\phi \left(c, \rho \right) = \frac{c}{1 + \lambda c^2} \left(\rho + \beta \nabla^2 \rho \right), \tag{2.4}$$

where the $\nabla^2 \rho$ term models the long-range traction effects that occur due to the fibrous nature of the ECM and β is a measure of the strength of the long-range traction force, while the λc^2 term models contact inhibition as the cell density increases.

The ECM is assumed to be passively convected by the displacement of the medium so, by conservation of mass,

$$\frac{\partial \rho}{\partial t} + \nabla \cdot \left(\rho \frac{\partial \boldsymbol{u}}{\partial t} \right) = 0. \tag{2.5}$$

In addition to the governing equations, appropriate boundary conditions are needed for the model to be well-posed. Appropriate choices for the force balance equation, (2.2), include periodic displacements and stress-free ($\boldsymbol{\sigma} = \mathbf{0}$) and pinned ($\boldsymbol{u} = \mathbf{0}$) boundary conditions. For the density equations, there are two choices that arise from the choice of frame of reference. Choosing the deformed frame of reference, there is no need for boundary conditions for the density equations. This approach was used for a variation of the OMH model by Moon and Tranquillo [16] in studying FPCMs. The disadvantage of this approach is the difficulty that arises from having to

incorporate the deformation of the domain in numerical simulations and also incorporating the deformations of the domain in the nonlinear analysis since the deformation of the domain is not known a priori.

To simplify both the analysis and numerics, one can impose the infinitesimal displacement assumption, taking the deformed and referenced domains to be equivalent, and use the governing equations on the static reference domain. In this case, boundary conditions need to be specified for the density equations for well-posedness. Since the density equations are purely hyperbolic, we do not have to specify a boundary condition where the normal velocity is positive ($\hat{\boldsymbol{n}} \cdot \partial \boldsymbol{u}/\partial t > 0$) on the boundary, where $\hat{\boldsymbol{n}}$ is the outward unit normal. When the normal velocity is negative ($\hat{\boldsymbol{n}} \cdot \partial \boldsymbol{u}/\partial t < 0$) we must specify an appropriate inflow boundary condition for both the cell and ECM densities. For periodic displacements, any outflowing boundary is mapped periodically to the appropriate inflow boundary. For pinned boundary conditions, there are no inflows or outflows since $\boldsymbol{u} = \boldsymbol{0}$, and consequently $\partial \boldsymbol{u}/\partial t = \boldsymbol{0}$ for all time. For stress-free boundary conditions, we are not so fortunate. Stress-free boundary conditions are the appropriate boundary conditions for unpinned FPCL and FPCM arrays, but for the OMH model as written, $\partial \boldsymbol{u}/\partial t \neq \boldsymbol{0}$ does not hold on the boundaries for all time, and so ECM can flow through the boundaries. Physically, we cannot have ECM entering or leaving the domain, so we are unable to specify appropriate boundary conditions on the cell/ECM densities if there are stress-free boundary conditions on the medium. This significantly reduces the possible experimental applications of the OMH model under the infinitesimal displacement assumption.

3. Modified Oster–Murray–Harris model. To correct the boundary condition issue, we will rederive the OMH model in the material frame of reference. For simplicity, the derivation is done in one dimension. The modified two-dimensional version can be found in Appendix B. As before, we focus only on the cell traction effects of fibroblasts on the ECM and neglect active fibroblast and ECM processes, such as cell growth/death, ECM production/degradation, chemotaxis, haptotaxis, cell diffusion, and contact guidance that could be included in the OMH model [17].

We begin by assuming that the cells are embedded in a moving medium in the deformed frame of reference and are governed only by advection. From conservation of mass, the governing equation for the cell density in the deformed frame is

$$\frac{\partial c}{\partial t} + \frac{\partial}{\partial \hat{x}}(vc) = 0, \tag{3.1}$$

where c and $\hat{x}$ are the cell density and the spatial coordinate in the deformed frame of reference, respectively, and v is the velocity of the medium. Since the cell density is governed solely by the advection of the medium, we can convert between the cell density in deformed coordinates and the cell density in reference coordinates using the relation $c_0 = Jc$, where c_0 is the cell density in reference coordinates, $J = 1 + \partial u/\partial x$ is the determinant of the deformation gradient tensor in one dimension, and x is the spatial coordinate in the undeformed frame of reference. Likewise, we can relate the ECM density in deformed coordinates to the ECM density in reference coordinates using a similar relation, $\rho_0 = J\rho$, where ρ_0 is the ECM density in the reference coordinates.

As with the OMH model, the ECM medium is assumed to be a viscoelastic medium. Our force balance equation in reference coordinates is

$$\rho_0 \frac{\partial^2 u}{\partial t^2} = \hat{\mu} \frac{\partial^3 u}{\partial t \partial x^2} + E(1+\nu') \frac{\partial^2 u}{\partial x^2} + \frac{\partial}{\partial x}\left[\hat{\tau}\phi(c,\rho)\right] - \hat{s}\rho_0 u, \tag{3.2}$$

where $\hat{\mu} = \hat{\mu}_1 + \hat{\mu}_2$. Note that we retain the inertial term, $\rho_0 \partial^2 u/\partial t^2$, which was ignored in the OMH model.

The $\hat{\tau}\phi(c,\rho)$ term is the traction force that depends on the cell and ECM densities in the deformed frame of reference. The long-range traction term in the traction force is also formulated in the deformed frame of reference, so we must convert this term to the reference frame. Taking the derivative of the definition of the displacement, $u = \hat{x}(x,t) - x$, with respect to the spatial coordinate in the reference frame, x, we obtain

$$\frac{\partial \hat{x}}{\partial x} = 1 + \frac{\partial u}{\partial x} = 1 + u_x. \tag{3.3}$$

Hence,

$$\frac{\partial}{\partial \hat{x}} = \frac{\partial x}{\partial \hat{x}}\frac{\partial}{\partial x} = \frac{1}{1+u_x}\frac{\partial}{\partial x}. \tag{3.4}$$

The traction force is now

$$\phi(c,\rho) = \phi(u_x) = \frac{c_0\rho_0}{(1+u_x)^2 + \hat{\lambda}c_0^2}\left(1 + \hat{\beta}\frac{\partial}{\partial x}\left[\frac{1}{1+u_x}\frac{\partial}{\partial x}\left(\frac{1}{1+u_x}\right)\right]\right). \tag{3.5}$$

We have removed the need for boundary conditions for the cell and ECM densities since the hyperbolic equations for the densities have been replaced with algebraic equations. We are now able to enforce boundary conditions other than pinned or periodic conditions. The simplification of the equations governing the cell and ECM densities comes at the cost of increasing the complexity of the traction force due to the conversion from the deformed frame to the reference frame.

Since the density equations are now algebraic, we need only specify boundary conditions for the force balance equation. Choices for boundary conditions include periodic, pinned ($u = 0$ on the boundary), no viscoelastic stress ($\sigma = 0$), and no viscoelastic stress or cell/ECM traction forces,

$$\hat{\mu}\frac{\partial^2 u}{\partial t \partial x} + E(1+\nu')\frac{\partial u}{\partial x} + \hat{\tau}\phi(u_x) = 0. \tag{3.6}$$

Note that the force balance equation is fourth order in space due to the long-range traction force, so two extra boundary conditions are needed in addition to the pinned or stress-free boundary conditions. Two such choices for the second condition are $\rho_x = 0$ (no net contribution to the total long-range traction force in the interior from the boundary) and $\rho_{xx} = 0$ (zero long-range traction forces on the boundary) on the boundary in the deformed frame, which translates to the conditions $u_{xx} = 0$ and $u_{xxx}(1+u_x) = 3u_{xx}^2$, respectively, in the reference frame. These boundary conditions are summarized in Table 3.1.

Using length scale L and time scale T, we obtain the dimensionless modified model in the reference frame:

$$\begin{aligned}\alpha\frac{\partial^2 u}{\partial t^2} = {} & \mu\frac{\partial^3 u}{\partial t \partial x^2} + \frac{\partial^2 u}{\partial x^2} - su \\ & + \tau\frac{\partial}{\partial x}\left(\frac{1}{(1+u_x)^2 + \lambda}\left[1 + \beta\frac{\partial}{\partial x}\left(\frac{1}{1+u_x}\frac{\partial}{\partial x}\left[\frac{1}{1+u_x}\right]\right)\right]\right),\end{aligned} \tag{3.7}$$

where $\alpha = \rho_0 L^2/\left(E(1+\nu')T^2\right)$, $\mu = \hat{\mu}/\left(E(1+\nu')T\right)$, $\tau = \hat{\tau}c_0\rho_0/\left(E(1+\nu')\right)$, $\lambda = \hat{\lambda}c_0^2$, $\beta = \hat{\beta}/L^2$, and $s = \hat{s}\rho_0 L^2$.

TABLE 3.1

Some possible boundary conditions for the modified OMH model, (3.2) *and* (3.5). *Since the modified model is a fourth-order system in space, we must enforce a total of four boundary conditions, two on the displacement and/or stress and two on the long-range traction force.*

Boundary conditions on the displacement/stress	
Type	Definition
Periodic	$u(0,t) = u(L,t)$
Pinned	$u = 0$
No viscoelastic stress	$u_t + E(1+\nu')u_x = 0$
No viscoelastic stress/traction forces	$\mu u_t + E(1+\nu')u_x + \hat{\tau}\phi(c,\rho) = 0$
Boundary conditions on the long-range traction force	
Type	Definition
$\rho_x = 0$	$u_{xx} = 0$
$\rho_{xx} = 0$	$u_{xxx}(1+u_x) = 3u_{xx}^2$

4. Linear analysis. We now examine the linear stability of the modified model. Note that since the differences between the original OMH model and the modified model are nonlinear, the linear analysis in the absence of inertial terms is the same in both models. We start by assuming small perturbations to the spatially uniform steady state $u = 0$, which yields the linearized equation

$$\alpha\frac{\partial^2 u}{\partial t^2} = \mu\frac{\partial^3 u}{\partial t \partial x^2} + \left(1 - 2\frac{\tau}{(1+\lambda)^2}\right)\frac{\partial^2 u}{\partial x^2} - \frac{\tau\beta}{1+\lambda}\frac{\partial^4 u}{\partial x^4} - su. \tag{4.1}$$

We assume periodic boundary conditions, noting that the bifurcation conditions are the same for pinned boundary conditions ($u = 0$ and $u_{xx} = 0$) and no viscous stress boundary conditions ($\sigma = 0$ and $u_{xxx} = 0$). Using the ansatz that the displacements are of the form $u \propto \exp\left(\omega\left(k^2\right)t + ikx\right)$, we have the characteristic equation

$$\alpha\omega^2 + \mu k^2\omega + B\left(k^2\right) = 0, \tag{4.2}$$

where

$$B\left(k^2\right) = \tau_\lambda\beta_\lambda k^4 + \left(1 - 2\tau_\lambda\right)k^2 + s, \tag{4.3}$$

$\tau_\lambda = \tau/(1+\lambda)^2$, and $\beta_\lambda = \beta(1+\lambda)$.

If we neglect inertia by assuming $\alpha = 0$, we recover the characteristic equation for the original OMH model,

$$\mu k^2\omega\left(k^2\right) + B\left(k^2\right) = 0, \tag{4.4}$$

whose solution is

$$\omega\left(k^2\right) = -\frac{B\left(k^2\right)}{\mu k^2}. \tag{4.5}$$

If $B\left(k^2\right) < 0$ for some k^2, then the uniform steady state is linearly unstable for small random perturbations, and we expect these small random perturbations to grow in time. A bifurcation to a spatial pattern with wavenumber k_c^2 occurs as τ_λ increases when

$$\tau_\lambda > \frac{1}{2} \quad \text{and} \quad \left(2\tau_\lambda - 1\right)^2 = 4\beta_\lambda\tau_\lambda s, \tag{4.6}$$

where the critical wavenumber is

$$k_c^2 = \sqrt{\frac{s}{\tau_\lambda \beta_\lambda}}. \tag{4.7}$$

Note that these are the same bifurcation conditions as in the original OMH model.

For $\alpha \neq 0$, there are two roots of the characteristic equation (4.2):

$$\omega\left(k^2\right) = \frac{1}{2\alpha}\left(-\mu k^2 \pm \sqrt{\mu^2 k^4 - 4\alpha B\left(k^2\right)}\right). \tag{4.8}$$

Here, one root always has a negative real part and the other can have a positive real part if $B\left(k^2\right) < 0$ for some k^2. Hence, we obtain the exact same bifurcation conditions as in the case without inertia ($\alpha = 0$) except that $\Im\left\{\omega\left(k^2\right)\right\}$ is not necessarily zero for all k^2.

5. Multiscale nonlinear analysis. To examine the behavior of the full nonlinear system near the bifurcation point, we perform a multiscale analysis on the modified model (3.7). This was done for the OMH model by Maini and Murray [15], and our analysis will be similar. This is a lengthy calculation, so we summarize the key results here, with a more detailed description of the analysis given in Appendix A. We will assume periodic boundary conditions in the analysis to match the work done by Maini and Murray [15].

We take τ as our bifurcation parameter in (3.7), and if τ is slightly larger than τ_c, where τ_c satisfies the bifurcation conditions, (4.6), the uniform steady state will be unstable to small random perturbations, and the fastest growing mode will be k_c, assuming k_c is an admissible mode. Hence, we set $\tau = \tau_c + \varepsilon^2\delta$ and assume a long time scale $T = \varepsilon^2 t$, where $\varepsilon \ll 1$ and $\delta = \pm 1$. We now expand u in a power series of ε to obtain a hierarchy of equations for each power of ε. By solving this hierarchy of equations, we obtain the Landau equation for the amplitude, $A(t)$, of the critical wavemode of u:

$$\mu k_c^2 \frac{\partial}{\partial T} A(T) = \delta X A(T) + Y A(T)^3. \tag{5.1}$$

The coefficients of the Landau equation are

$$X = \frac{k_c^2}{(1+\lambda)^2}\frac{2\tau_{\lambda_c} + 1}{2\tau_{\lambda_c}} \tag{5.2}$$

and

$$Y = \frac{k_c^4\left[(344\lambda^2 - 4\lambda + 20)\tau_{\lambda_c}^2 - (192\lambda^2 + 532\lambda + 212)\tau_{\lambda_c} + 18\lambda^2 + 219\lambda + 173\right]}{72\left(2\tau_{\lambda_c} - 1\right)(1+\lambda)^2}, \tag{5.3}$$

where $\tau_{\lambda_c} = \tau_c/\left(1+\lambda^2\right)$. Since $X > 0$ and assuming $\delta = 1$, the Landau equation predicts that the amplitude $A(t)$ of the critical wavemode will evolve to a bounded steady state when $Y < 0$. Hence,

$$A(t) \to \pm\sqrt{\frac{X}{|Y|}} \quad \text{as } t \to \infty. \tag{5.4}$$

We can compare this result with the result from the original OMH model [15] by setting $\lambda = 0$. The coefficients of the Landau equation are now

$$X = k_c^2 \frac{2\tau_c + 1}{2\tau_c} \tag{5.5}$$

and

$$Y = \frac{k_c^4}{72} \frac{20\tau_c^2 - 212\tau_c + 173}{2\tau_c - 1}. \tag{5.6}$$

Since $\tau_c = (1+\beta s+\sqrt{\beta s\,(2+\beta s)})/2$ from the bifurcation conditions, we can plot the region in β-s parameter space where the nonlinear analysis suggests that the system evolves to a bounded steady state when $\delta = 1$, which is shown in Figure 5.1. Note that the bounded region for the original OMH model I is a subset of the bounded region of the updated model (entire shaded region). Relaxing the assumptions made on displacements in the original OMH model greatly increases the region in parameter space where the nonlinear analysis suggests that the solution will evolve to a bounded steady state.

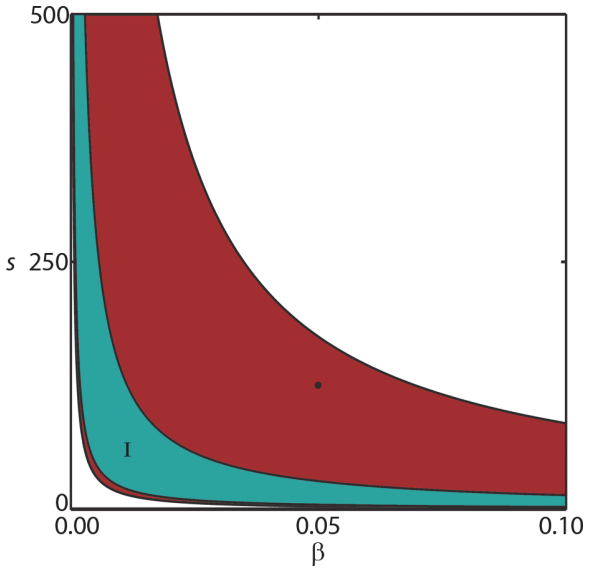

FIG. 5.1. *Regions in β-s parameter space where the nonlinear analysis predicts that the solution will evolve to a bounded steady state for the original* I *and modified OMH model (entire shaded region). Values of β and s within the shaded region yield bounded solutions as $t \to \infty$. We can see that the region for the original OMH model is a subset of the region for the modified model. The dot corresponds to the values of β and s used in Figure* 6.3.

If $\lambda \neq 0$, the region in β-s parameter space where the nonlinear analysis predicts that the solution will evolve to a bounded steady state changes with λ. To better illustrate this, we plot the region in λ-τ_c space, which is shown in Figure 5.2. Here, each value of τ_c on the boundary corresponds to a hyperbola in β-s space for a given λ. As λ increases, there is an initial increase in the range of τ_c for which the solution will evolve to a bounded steady state until it reaches a maximum for $\lambda \approx 0.1417$, after which the range of τ_c decreases. For $\lambda > 3.5233$, the solution is predicted to grow unbounded for any value of τ_c, and hence β and s.

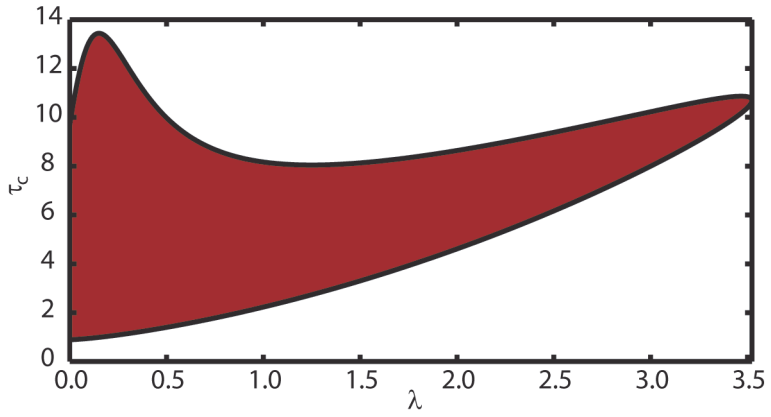

FIG. 5.2. *Region in λ-τ_c parameter space where the solution to the modified model is predicted by nonlinear analysis to evolve to a bounded steady state. Values of λ and τ_c within the shaded region yield bounded solutions.*

6. One-dimensional numerical results. To investigate the behavior of the full nonlinear system and to verify the results from the multiscale nonlinear analysis, we perform numerical simulations in one dimension on the full nonlinear system, (3.4) and (3.5), using the finite difference method in space and an adaptive, multistep implicit method in time [28]. The length of the domain in each simulation is 2π, and we enforce periodic boundary conditions on the ends of the domain. The uniform initial condition, $u = 0$, is perturbed at each grid point by a random value chosen from a uniform random distribution with zero mean and a standard deviation of $\sqrt{3}/3 \times 10^{-5}$. We filter out the $k^2 = 0$ mode from the perturbations to remove any initial rigid body translation of the reference frame, which prevents the oscillating translations predicted by the linear analysis.

Figure 6.1 shows the numerical steady state solution near the bifurcation point where the critical wavemode is $k_c = 3$ with $\tau_c = 1$ and $\varepsilon = 10^{-1}$. The amplitude of this mode in the numerical steady state solution is 7.67×10^{-2}, and the amplitude of the critical wavemode predicted by the multiscale nonlinear analysis for these parameters is 7.95×10^{-2}.

Figure 6.2 shows the numerical steady state solution near the bifurcation point with $\lambda \neq 0$, where the critical wavemode is $k_c = 4$ with $\tau_c = 169/100$ and $\varepsilon = 10^{-1}$. The amplitude of this mode is 2.51×10^{-2}, and the amplitude of the critical wavemode predicted by the multiscale nonlinear analysis for these parameters is 2.61×10^{-2}. We can see in both the $k_c = 3$ and $k_c = 4$ cases that there is good agreement between the results from the numerical simulations and the multiscale nonlinear analysis.

To see the effect of α and μ on the steady state, we numerically solved the equations for varying α and μ with τ, β, λ, and s held the same as those used in (6.2), and we compared the steady state solution with the solution for $\alpha = \mu = 1$. For fixed τ, λ, β, and s, there is no change in the steady state solution for α and μ. This matches the assumptions and predictions from the multiscale nonlinear analysis.

We additionally compare the long time behavior of the original OMH model with the modified model for the same parameters. In Figure 6.3, the minimum dilation ($\min u_x$) in the domain is plotted versus time for both the OMH model and the modified model. The parameters are the same for both simulations and are chosen such

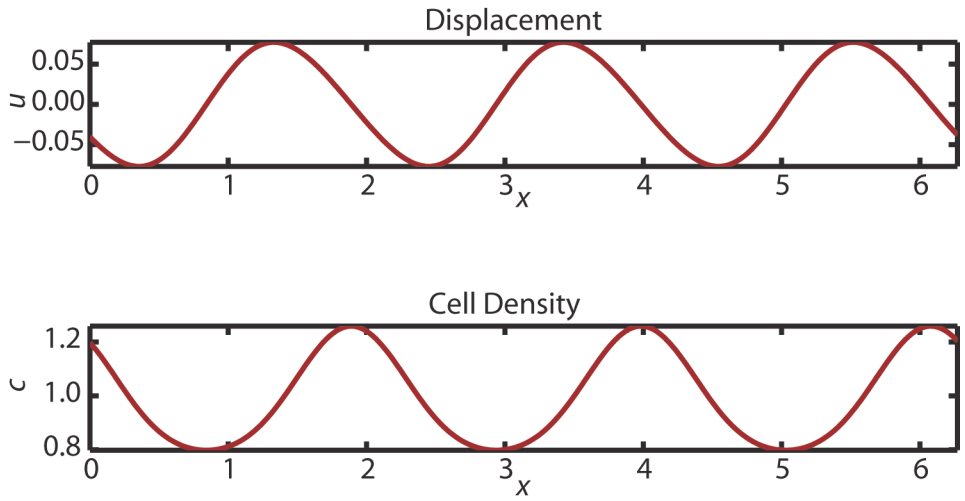

FIG. 6.1. *Numerically calculated steady state solution of* (3.7) *when* $\lambda = 0$, $\tau = 101/100$, $\beta = 1/18$, $s = 9/2$, $\alpha = 1$, *and* $\mu = 1$ *with* $k_c = 3$, $\tau_c = 1$, *and* $\varepsilon = 10^{-1}$. *The cell density is computed using the relation* $c = J^{-1}c_0 = c_0/(1 + u_x)$. *The amplitude of this wavemode predicted by the analysis is* 7.95×10^{-2} *and is found from our numerical simulations to be* 7.67×10^{-2}.

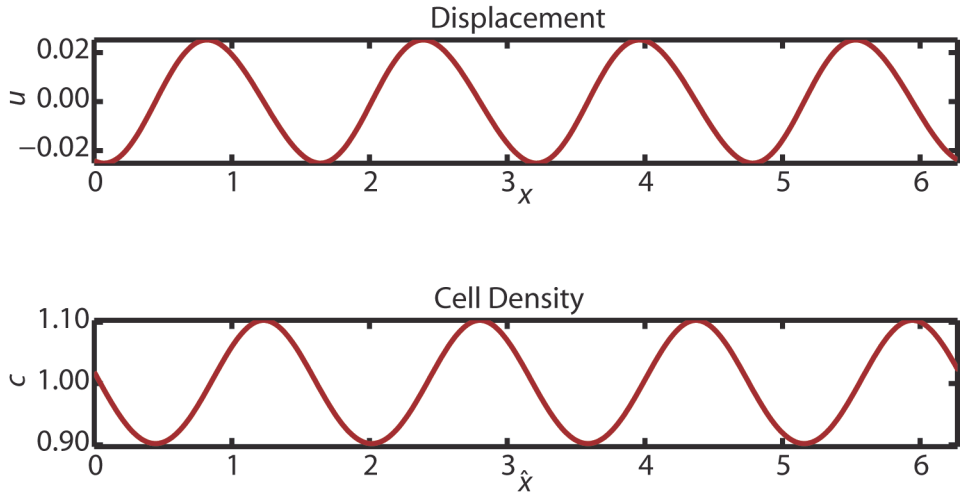

FIG. 6.2. *Numerically calculated steady state solution of* (3.7) *when* $\lambda = 3/10$, $\tau = 17/10$, $\beta = 5/208$, $s = 8$, $\alpha = 1$, *and* $\mu = 1$ *with* $k_c = 4$, $\tau_c = 169/100$, *and* $\varepsilon = 10^{-1}$. *The cell density is computed using the relation* $c = J^{-1}c_0 = c_0/(1 + u_x)$. *The amplitude of this wavemode predicted by the analysis is* 2.61×10^{-2} *and is found from our numerical simulations to be* 2.51×10^{-2}.

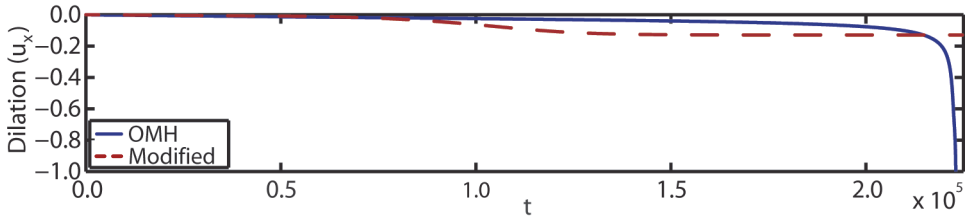

FIG. 6.3. *A comparison of the minimum dilation* ($\min u_x$) *in the domain versus time for the original OMH model,* (2.1)–(2.5)*, and the modified model introduced in section* 3*,* (3.7)*. The parameters in these simulations are chosen to be near the bifurcation point and to lie outside the bounded region in* β*-*s *parameter space for the OMH model but within the bounded region for the modified model, as shown by the dot in Figure* 5.1*. This is a typical simulation and illustrates the increase in the range of parameters where the modified model can exhibit bounded solutions, according to the nonlinear analysis. Note that the simulation is stopped when* $u_x = -1$ *in the OMH simulation. This is because the solution for* $u_x \leq -1$ *violates the impenetrability condition of the material, and the model is no longer valid. The parameters are* $\alpha = 1$ *(for the modified model),* $\mu = 100$*,* $\tau = 8.3122 + \varepsilon^2$*,* $s = 125$*,* $\beta = 5.8738 \times 10^{-2}$*,* $\lambda = 0$*, and* $\varepsilon^2 = 5 \times 10^{-3}$*. The magnitude of the initial perturbation is* 10^{-5}*, and the magnitude of the steady state solution predicted for the modified model is* 4.24×10^{-2}*, which is in good agreement with the numerical solution,* 3.76×10^{-2}*.*

that the uniform steady state is linearly unstable with the long time solution predicted by multiscale nonlinear analysis unbounded for the OMH model and bounded for the modified model. This illustrates that the approximations made in the original derivation can greatly restrict the range of parameters for which the model is valid. This restriction can be eased by using the modified derivation proposed in section 3. Note that the simulation is stopped when $u_x = -1$ in the OMH simulation. This is because the solution for $u_x \leq -1$ violates the impenetrability condition of the material, and the model is no longer valid.

7. Two-dimensional numerical results. The simulations in the previous section were performed in one dimension on a periodic domain. In this section, we will give numerical results in two dimensions using stress-free boundary conditions. We solve the dimensionless small strain approximation given in Appendix B:

$$\alpha \frac{\partial^2 \theta}{\partial t^2} = \mu \frac{\partial}{\partial t} \nabla^2 \theta + \nabla^2 \theta + \tau \nabla^2 \phi - s\theta, \tag{7.1}$$

where

$$\phi(\theta) = \frac{1}{(1+\theta)^2 + \lambda} \left(1 + \beta \nabla \cdot \left[\frac{1}{1+\theta} \nabla \left(\frac{1}{1+\theta} \right) \right] \right). \tag{7.2}$$

In this section, we enforce stress-free boundary conditions of the form

$$\hat{\boldsymbol{n}} \cdot \nabla \left(\mu \frac{\partial \theta}{\partial t} + \theta + \tau \phi \right) = 0 \tag{7.3}$$

and

$$\hat{\boldsymbol{n}} \cdot \nabla \theta = 0. \tag{7.4}$$

The domain is $2\pi \times 2\pi$ in each simulation. The small strain approximation is discretized using the finite element method where the domain is meshed using 100×100

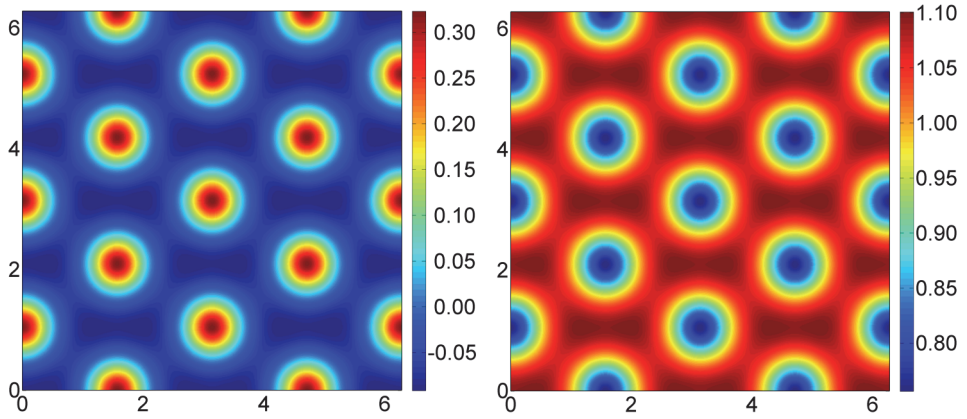

(a) Dilation. (b) Cell/ECM density.

FIG. 7.1. *Steady state dilation θ (left) and the nondimensional cell density c (right) of* (B.8) *and* (B.9). *The parameters are $\alpha = 10^{-4}$, $\mu = 1$, $s = 7$, $\beta = 7/351$, $\mu = 1$, and $\tau = 4.158$ on a $2\pi \times 2\pi$ domain. The only linearly growing admissible wavenumber is $k_c^2 = 13$, which matches the dominant $(2, 3)$ wavemode in the steady state hexagonal pattern.*

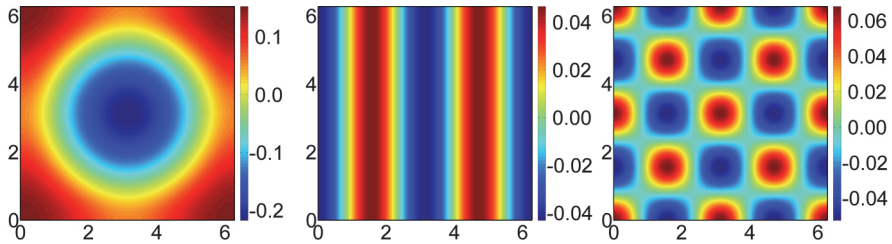

(a) $k_c^2 = 1$. (b) $k_c^2 = 4$. (c) $k_c^2 = 8$.

FIG. 7.2. *Numerical steady state solutions for the dilation of* (B.8) *and* (B.9) *on a $2\pi \times 2\pi$ domain with stress-free conditions enforced on the boundaries. The dominant wavemodes in each simulation correspond to the admissible wavemodes predicted by the linear stability analysis with* (a) *exhibiting a linear combination of the $(1, 0)$ and $(0, 1)$ modes, the $(2, 0)$ mode dominant in* (b), *and the $(2, 2)$ mode dominant in* (c). *The parameters are $\alpha = 10^{-4}$, $\mu = 1$, and $\lambda = 1$ in all three cases. For* (a), *$s = 1/10$, $\beta = 1/12$, and $\tau = 2.4024$. For* (b), *$s = 1$, $\beta = 1/24$, and $\tau = 3.003$. For* (c), *$s = 3$, $\beta = 3/112$, and $\tau = 3.5035$.*

regular biquadratic elements ($h = 0.063$ for a $2\pi \times 2\pi$ domain). The semidiscretized nonlinear equations are then integrated in time using a variable-order variable-stepsize backwards difference formula solver [12]. The simulations are run until $\max |d\theta/dt| < 10^{-8}$.

Figure 7.1 shows the steady state dilation, θ, and the nondimensional cell density, c. Note that the nondimensional ECM density is equal to the nondimensional cell density. The dominant wavemode predicted by the one-dimensional linear stability analysis is $k_c^2 = 13$, which matches the dominant (2,3) wavemode in the steady state hexagonal pattern. Note that minima of the dilation correspond to maxima in the cell density. Figure 7.2 shows the steady state dilation for various critical wavemodes, k_c^2. We can see in Figures 7.1 and 7.2 that the patterning exhibits stripe, square, and hexagonal patterns. Due to the degeneracy that is inherent in two dimensions, in each case the steady state solution depends on the initial conditions.

8. Conclusions. The OMH model is an alternative morphogenic model which considers the role of mechanical forces during morphogenesis. A limitation of the original formulation of the OMH model is that there is a restriction on the range of well-posed boundary conditions, especially when trying to apply stress-free conditions on the boundary. In this paper, we rederive the OMH model while preserving the appropriate frames of reference. This allows for the use of stress-free boundary conditions as well as pinned and periodic conditions.

We performed linear and multiscale nonlinear analysis on the modified model and compared the results to the original OMH model. The bifurcation conditions from linear analysis are equivalent, while the nonlinear analysis predicts that the modified model has an increased range of parameters where the solution is predicted to evolve to a bounded steady state.

Numerical simulations of the full nonlinear model performed in one dimension confirm the predictions from the linear and nonlinear analysis, verifying the use of the analysis for predicting the behavior of the full nonlinear model. Two-dimensional simulations were performed for stress-free boundary conditions and exhibit a wide variety of patterns.

In the future, we will expand this modified model to include active cell/ECM effects as well as mechanochemical interactions among fibroblasts, ECM, and various chemical promoters/inhibitors. Using modeling along with analytic and numerical methods, we hope to shed light on how various mechanisms contribute to the patterning process and to validate and predict experimental results.

Appendix A. Derivation of the Landau equation. To examine the behavior of the full nonlinear system near the bifurcation point, we perform a multiscale analysis on the modified model (3.7). This was done for the OMH model by Maini and Murray [15], and our analysis will be similar. To match the previous work by Maini and Murray, we will assume periodic boundary conditions in the analysis.

We start by transforming (3.7) into a system of equations by letting $v = \partial u/\partial t$, which yields

$$\frac{\partial u}{\partial t} = v \tag{A.1}$$

and

$$\alpha\frac{\partial v}{\partial t} = \mu\frac{\partial^2 v}{\partial x^2} + \frac{\partial^2 u}{\partial x^2} + \tau\frac{\partial}{\partial x}\left(\frac{1}{(1+u_x)^2}\left[1+\beta\frac{\partial}{\partial x}\left(\frac{1}{1+u_x}\frac{\partial}{\partial x}\left[\frac{1}{1+u_x}\right]\right)\right]\right) - su. \tag{A.2}$$

We again take τ as our bifurcation parameter and set $\tau = \tau_c + \varepsilon^2\delta$. We assume a long time scale, $T = \varepsilon^2 t$, where $\varepsilon \ll 1$ and $\delta = \pm 1$. We now expand u and v in power series of ε:

$$u(x,T) = \sum_{j=1}^{\infty}\frac{\varepsilon^j}{j!}u_i(x,T) \quad \text{and} \quad v(x,T) = \sum_{j=1}^{\infty}\frac{\varepsilon^j}{j!}v_i(x,T). \tag{A.3}$$

Substituting (A.3) into (A.1) and (A.2) and balancing powers of ε, we obtain a hierarchy of equations for each power of ε.

The $\mathcal{O}(\varepsilon)$ equations are $v_1 \equiv 0$ and

$$\frac{\tau_c \beta}{1+\lambda}\frac{\partial^4 u_1}{\partial x^4} - \left(1 - \frac{2\tau_c}{(1+\lambda)^2}\right)\frac{\partial^2 u_1}{\partial x^2} + s u_1 = 0. \tag{A.4}$$

We define $\tau_{\lambda_c} = \tau_c/(1+\lambda)^2$ and $\beta_\lambda = \beta(1+\lambda)$, so (A.4) reduces to

$$L(u_1) = \tau_{\lambda_c}\beta_\lambda \frac{\partial^4 u_1}{\partial x^4} - (1 - 2\tau_{\lambda_c})\frac{\partial^2 u_1}{\partial x^2} + s u_1 = 0, \tag{A.5}$$

where $L(u)$ is a linear differential operator. We assume that u_j can be expanded in a Fourier series with general form

$$u_j(x,T) = A_{0,(j-1)}(T) + \sum_{n=1}^{\infty}\left[A_{n,(j-1)}(T)\cos(nk_c x) + B_{n,(j-1)}(T)\sin(nk_c x)\right]. \tag{A.6}$$

Substituting (A.6) into (A.5), equating harmonics, and using the definition of k_c from (4.7), we get $A_{n,0}(T) \equiv 0$ and $B_{n,0}(T) \equiv 0$ for $n \neq 1$ with $A_{1,0}(T)$ and $B_{1,0}(T)$ to be determined from the higher order equations. Hence,

$$u_1(x,T) = A_{1,0}(T)\cos(k_c x) + B_{1,0}(T)\sin(k_c x). \tag{A.7}$$

The $\mathcal{O}(\varepsilon^2)$ equations are $v_2 \equiv 0$ and

$$\begin{aligned} L(u_2) = {} & 2\tau_{\lambda_c}\left(\frac{3-\lambda}{1+\lambda}\right)\frac{\partial u_1}{\partial x}\frac{\partial^2 u_1}{\partial x^2} \\ & + \tau_{\lambda_c}\beta_\lambda\left[\left(\frac{5+3\lambda}{1+\lambda}\right)\frac{\partial u_1}{\partial x}\frac{\partial^4 u_1}{\partial x^4} + \left(\frac{11+9\lambda}{1+\lambda}\right)\frac{\partial^2 u_1}{\partial x^2}\frac{\partial^3 u_1}{\partial x^3}\right]. \end{aligned} \tag{A.8}$$

Substituting (A.6) and (A.7) into (A.8) and equating harmonics, we get $A_{n,1}(T) \equiv 0$ and $B_{n,1}(T) \equiv 0$ for $n \neq 1, 2$. For $n = 1$, (A.8) is automatically satisfied, with $A_{1,1}(T)$ and $B_{1,1}(T)$ being undetermined. Solving (A.8) for $n = 2$ yields

$$A_{2,1}(T) = 2\gamma_\lambda A_{1,0}(T) B_{1,0}(T) \tag{A.9}$$

and

$$B_{2,1}(T) = -\gamma_\lambda\left(A_{1,0}(T)^2 - B_{1,0}(T)^2\right), \tag{A.10}$$

where

$$\gamma_\lambda = \frac{\tau_\lambda k_c^3}{B(4k_c^2)}\left(2\left(\frac{4+3\lambda}{1+\lambda}\right)\beta_\lambda k_c^2 - \left(\frac{3-\lambda}{1+\lambda}\right)\right), \tag{A.11}$$

with $B(k^2)$ defined as in (4.3).

The $\mathcal{O}(\varepsilon^3)$ equations are

$$v_3 = \frac{\partial u_1}{\partial T} \tag{A.12}$$

and

$$\mu\frac{\partial^2 v_3}{\partial x^2} = L(u_3) + \frac{\delta}{(1+\lambda)^2}\left(2\frac{\partial u_1}{\partial x} + \beta_\lambda \frac{\partial^4 u_1}{\partial x^4}\right) + \frac{\tau_{\lambda_c}}{1+\lambda}N(u_1, u_2), \tag{A.13}$$

where

$$\begin{aligned} N(u_1,u_2) = {} & 12(1-\lambda)\frac{\partial^2 u_1}{\partial x^2}\left(\frac{\partial u_1}{\partial x}\right)^2 - 2\left(3+2\lambda-\lambda^2\right)\frac{\partial}{\partial x}\left(\frac{\partial u_1}{\partial x}\frac{\partial u_2}{\partial x}\right) \\ & + \frac{\beta_\lambda}{1+\lambda}\left[2\left(33+47\lambda+18\lambda^2\right)\frac{\partial u_1}{\partial x}\frac{\partial^2 u_1}{\partial x^2}\frac{\partial^3 u_1}{\partial x^3}\right. \\ & - \left(5+8\lambda+3\lambda^2\right)\left(\frac{\partial u_1}{\partial x}\frac{\partial^4 u_2}{\partial x^4} + \frac{\partial u_2}{\partial x}\frac{\partial^4 u_1}{\partial x^4}\right) \\ & - \left(11+20\lambda+9\lambda^2\right)\left(\frac{\partial^2 u_1}{\partial x^2}\frac{\partial^3 u_2}{\partial x^3} + \frac{\partial^2 u_2}{\partial x^2}\frac{\partial^3 u_1}{\partial x^3}\right) \\ & \left. + \left(15+17\lambda+6\lambda^2\right)\frac{\partial^4 u_1}{\partial x^4}\left(\frac{\partial u_1}{\partial x}\right)^2 + 6\left(3+5\lambda+2\lambda^2\right)\left(\frac{\partial^2 u_1}{\partial x^2}\right)^3\right]. \end{aligned} \tag{A.14}$$

Substituting (A.6), (A.7), (A.9), (A.10), and (A.12) into (A.13) and suppressing secular terms yields

$$\mu k_c^2\frac{\partial}{\partial T}A_{1,0}(T) = \delta X A_{1,0}(T) + Y A_{1,0}(T)\left(A_{1,0}(T)^2 + B_{1,0}(T)^2\right) \tag{A.15}$$

and

$$\mu k_c^2\frac{\partial}{\partial T}B_{1,0}(T) = \delta X B_{1,0}(T) + Y B_{1,0}(T)\left(A_{1,0}(T)^2 + B_{1,0}(T)^2\right), \tag{A.16}$$

where

$$X = \frac{k_c^2}{(1+\lambda)^2}\left(\beta_\lambda k_c^2 - 2\right) \tag{A.17}$$

and

$$\begin{aligned} Y = {} & \frac{k_c^4\tau_{\lambda_c}}{(1+\lambda)^2}\left[\frac{3}{4}\left(9+7\lambda+2\lambda^2\right)\beta_\lambda k_c^2 + 3(1-\lambda)\right. \\ & \left. - \frac{\tau_{\lambda_c}k_c^2}{B\left(4k_c^2\right)}\left[\left(13+3\lambda\right)\beta_\lambda k_c^2 - 3(3-\lambda)\right]\left[2(4+3\lambda)\beta_\lambda k_c^2 - (3-\lambda)\right]\right]. \end{aligned} \tag{A.18}$$

Multiplying (A.15) by $A_{1,0}(T)$, (A.16) by $B_{1,0}(T)$, and adding yields the Landau equation for the amplitude, $A(T)^2 = A_{1,0}(T)^2 + B_{1,0}(T)^2$,

$$\mu k_c^2\frac{\partial}{\partial T}A(T) = \delta X A(T) + Y A(T)^3. \tag{A.19}$$

We can simplify the above expressions for X and Y using the bifurcation conditions. We begin by writing

$$\beta_\lambda k_c^2 = \sqrt{\frac{\beta_\lambda s}{\tau_{\lambda_c}}} = \frac{2\tau_{\lambda_c} - 1}{2\tau_{\lambda_c}} \tag{A.20}$$

using the bifurcation conditions (4.6). This allows us to simplify X to

$$X = \frac{k_c^2}{(1+\lambda)^2}\frac{2\tau_{\lambda_c}+1}{2\tau_{\lambda_c}} > 0. \tag{A.21}$$

Next, we note that

$$B\left(k_c^2\right) = \beta_\lambda \tau_{\lambda_c} k_c^4 - \left(2\tau_{\lambda_c}-1\right)k_c^2 + s = 0, \tag{A.22}$$

so by the definitions of τ_{λ_c} and k_c^2, we obtain

$$B\left(4k_c^2\right) = 16\beta_\lambda \tau_{\lambda_c} k_c^4 - 4\left(2\tau_{\lambda_c}-1\right)k_c^2 + s = 15\beta_\lambda \tau_{\lambda_c} k_c^4 - 3\left(2\tau_{\lambda_c}-1\right)k_c^2. \tag{A.23}$$

Using the bifurcation condition (4.6) and the definition of the critical wavemode (4.7), we obtain

$$\beta_\lambda \tau_{\lambda_c} k_c^4 = s \quad \text{and} \quad \left(2\tau_{\lambda_c}-1\right)k_c^2 = 2s, \tag{A.24}$$

and (A.23) reduces to

$$B\left(4k_c^2\right) = 15\beta_\lambda \tau_{\lambda_c} - 3\left(2\tau_{\lambda_c}-1\right)k_c^2 = 9s. \tag{A.25}$$

From the definition of k_c^2 in (4.7) and (A.20), (A.25) can be rewritten as

$$B\left(4k_c^2\right) = 9\beta_\lambda \tau_{\lambda_c} k_c^4 = \frac{9k_c^2}{2}\left(2\tau_{\lambda_c}-1\right). \tag{A.26}$$

Using (A.20) and (A.25), Y becomes

$$\begin{aligned} Y = \frac{k_c^4 \tau_{\lambda_c}}{(1+\lambda)^2}\Bigg[&\frac{3}{4}\left(9+7\lambda+2\lambda^2\right)\left(\frac{2\tau_{\lambda_c}-1}{2\tau_{\lambda_c}}\right) + 3\left(1-\lambda\right) \\ &- \frac{2\tau_{\lambda_c}}{9\left(2\tau_{\lambda_c}-1\right)}\left[\left(13+3\lambda\right)\left(\frac{2\tau_{\lambda_c}-1}{2\tau_{\lambda_c}}\right) - 3\left(3-\lambda\right)\right] \\ &\times\left[2\left(4+3\lambda\right)\left(\frac{2\tau_{\lambda_c}-1}{2\tau_{\lambda_c}}\right) - \left(3-\lambda\right)\right]\Bigg]. \end{aligned} \tag{A.27}$$

Factoring out k_c^4 and finding a common denominator, (A.27) simplifies to

$$Y = \frac{k_c^4\left[\left(344\lambda^2-4\lambda+20\right)\tau_{\lambda_c}^2 - \left(192\lambda^2+532\lambda+212\right)\tau_{\lambda_c} + \left(18\lambda^2+219\lambda+173\right)\right]}{72\left(2\tau_{\lambda_c}-1\right)\left(1+\lambda\right)^2}. \tag{A.28}$$

Appendix B. Two-dimensional derivation. In two dimensions, we follow the same procedure as for the derivation of the original OMH model except that we transform the cell/ECM conservation equations into the reference frame. Hence, $c_0 = Jc$ where c is the cell density in the deformed frame of reference, c_0 is the constant cell density in the reference frame, and J is the determinant of the deformation gradient tensor,

$$\mathbf{F} = \begin{bmatrix} 1+\dfrac{\partial u_1}{\partial x} & \dfrac{\partial u_1}{\partial y} \\ \dfrac{\partial u_2}{\partial x} & 1+\dfrac{\partial u_2}{\partial y} \end{bmatrix}, \tag{B.1}$$

where u_1 is the displacement in the x-direction and u_2 is the displacement in the y-direction. Likewise, we can relate the ECM density in deformed coordinates with the ECM density in reference coordinates using a similar relation, $\rho_0 = J\rho$, where ρ is the ECM density in the deformed frame and ρ_0 is the ECM density in the reference frame.

The force balance equation for the ECM medium in reference coordinates is

$$\rho_0 \frac{\partial^2 \boldsymbol{u}}{\partial t^2} = \nabla \cdot \left(\boldsymbol{\sigma} + \hat{\tau}\phi\left(c,\rho\right)\mathbf{I}\right) - \rho_0 \boldsymbol{B}, \tag{B.2}$$

where $\boldsymbol{\sigma}$ is the stress tensor, $\hat{\tau}\phi\left(c,\rho\right)$ is the traction force exerted by the cells, $\mathbf{I}$ is the identity tensor, and $\boldsymbol{B}$ represents the body forces. We assume that the body force is Hookean so $\boldsymbol{B} = \hat{s}\boldsymbol{u}$, where $\hat{s}$ is the spring constant. As with the one-dimensional derivation, we assume the stress tensors in reference and deformed coordinates are approximately equal so

$$\boldsymbol{\sigma} = \underbrace{\mu_1 \frac{\partial \boldsymbol{e}}{\partial t} + \mu_2 \frac{\partial \theta}{\partial t}\mathbf{I}}_{\text{viscous damping forces}} + \underbrace{E\left(\boldsymbol{e} + \nu'\theta\mathbf{I}\right)}_{\text{elastic forces}}, \tag{B.3}$$

where μ_1 and μ_2 are the shear and bulk viscosities, respectively, $\boldsymbol{e} = \left(\nabla\boldsymbol{u} + \nabla\boldsymbol{u}^T\right)/2$ is the linear strain tensor, $\theta = \nabla \cdot \boldsymbol{u}$ is the dilation, E is the Young's modulus, and $\nu' = \nu/\left(1-2\nu\right)$, where ν is the Poisson ratio. Again we will assume a simple form for the traction force:

$$\phi\left(c,\rho\right) = \frac{c}{1+\hat{\lambda}c^2}\left(\rho + \hat{\beta}\hat{\nabla}^2\rho\right). \tag{B.4}$$

Since the traction force (B.4) depends on the cell and ECM densities in the deformed frame, we transform them using the definitions $c = J^{-1}c_0$, $\rho = J^{-1}\rho_0$, and $\hat{\nabla} = \mathbf{F}^{-1}\nabla$ to obtain

$$\phi = \frac{J^{-1}c_0}{1+\hat{\lambda}\left(J^{-1}c_0\right)^2}\left(J^{-1}\rho_0 + \hat{\beta}\left(\mathbf{F}^{-1}\nabla\right)\cdot\left[\left(\mathbf{F}^{-1}\nabla\right)\left(J^{-1}\rho_0\right)\right]\right). \tag{B.5}$$

We can reduce the complexity of (B.5) by assuming small strains taking $J \approx 1+\theta$ and $\mathbf{F} \approx J^{-1}\mathbf{I}$ to obtain

$$\phi\left(\theta\right) = \frac{c_0}{\left(1+\theta\right)^2 + \hat{\lambda}c_0^2}\left(\rho_0 + \hat{\beta}\nabla\cdot\left[\frac{1}{1+\theta}\nabla\left(\frac{\rho_0}{1+\theta}\right)\right]\right). \tag{B.6}$$

If we take the divergence of (B.2) and couple it with the small strain traction force (B.6), we obtain the small strain approximation for the dilation, θ:

$$\rho_0 \frac{\partial^2\theta}{\partial t^2} = \hat{\mu}\frac{\partial}{\partial t}\nabla^2\theta + E\left(1+\nu'\right)\nabla^2\theta + \hat{\tau}\nabla^2\phi - \hat{s}\theta. \tag{B.7}$$

If we nondimensionalize the small strain approximation using the same scales used in section 3, we obtain the dimensionless small strain approximation:

$$\alpha\frac{\partial^2\theta}{\partial t^2} = \mu\frac{\partial}{\partial t}\nabla^2\theta + \nabla^2\theta + \tau\nabla^2\phi - s\theta, \tag{B.8}$$

where

$$\phi\left(\theta\right) = \frac{1}{\left(1+\theta\right)^2 + \lambda}\left(1 + \beta\nabla\cdot\left[\frac{1}{1+\theta}\nabla\left(\frac{1}{1+\theta}\right)\right]\right). \tag{B.9}$$

Acknowledgment. The authors would like to thank Dr. Cameron Hall for his helpful insights.

REFERENCES

[1] V. H. Barocas, A. G. Moon, and R. T. Tranquillo, *The fibroblast-populated collagen microsphere assay of cell traction force—part* 2*: Measurement of the cell traction parameter*, J. Biomech. Eng., 117 (1995), pp. 161–170.

[2] V. H. Barocas and R. T. Tranquillo, *A finite element solution for the anisotropic biphasic theory of tissue-equivalent mechanics: The effect of contact guidance on isometric cell traction measurement*, J. Biomech. Eng., 119 (1997), pp. 261–268.

[3] V. H. Barocas and R. T. Tranquillo, *An anisotropic biphasic theory of tissue-equivalent mechanics: The interplay among cell traction, fibrillar network deformation, fibril alignment, and cell contact guidance*, J. Biomech. Eng., 119 (1997), pp. 137–145.

[4] D. E. Bentil and J. D. Murray, *Pattern selection in biological pattern formation mechanisms*, Appl. Math. Lett., 4 (1991), pp. 1–5.

[5] D. E. Bentil and J. D. Murray, *On the mechanical theory for biological pattern formation*, Phys. D, 63 (1993), pp. 161–190.

[6] G. C. Cruywagen, P. K. Maini, and J. D. Murray, *Sequential pattern formation in a model for skin morphogenesis*, Math. Med. Biol., 9 (1992), pp. 227–248.

[7] G. C. Cruywagen and J. D. Murray, *On a tissue interaction model for skin pattern formation*, J. Nonlinear Sci., 2 (1992), pp. 217–240.

[8] J. C. Dallon and H. P. Ehrlich, *A review of fibroblast-populated collagen lattices*, Wound Repair Regen., 16 (2008), pp. 472–479.

[9] I. Ferrenq, L. Tranqui, B. Vailhe, P. Y. Gumery, and P. Tracqui, *Modelling biological gel contraction by cells: Mechanocellular formulation and cell traction force quantification*, Acta Biotheor., 45 (1997), pp. 267–293.

[10] S. J. Gilmore, B. L. Vaughan, A. Madzvamuse, and P. K. Maini, *A mechanochemical model of striae distensae*, Math Biosci., 240 (2012), pp. 141–147.

[11] A. K. Harris, P. Warner, and D. Stopak, *Generation of spatially periodic patterns by a mechanical instability: A mechanical alternative to the Turing model*, Development, 80 (1984), pp. 1–20.

[12] A. C. Hindmarsh, P. N. Brown, K. E. Grant, S. L. Lee, R. Serban, D. E. Shumaker, and C. S. Woodward, *Sundials: Suite of nonlinear and differential/algebraic equation solvers*, ACM Trans. Math. Software, 31 (2005), pp. 363–396.

[13] L. Landau and E. Lifshitz, *Theory of Elasticity*, 2nd ed., Pergamon Press, London, 1970.

[14] M. A. Lewis and J. D. Murray, *Analysis of stable two-dimensional patterns in contractile cytogel*, J. Nonlinear Sci., 1 (1991), pp. 289–311.

[15] P. K. Maini and J. D. Murray, *A nonlinear analysis of a mechanical model for biological pattern formation*, SIAM J. Appl. Math., 48 (1988), pp. 1064–1072.

[16] A. G. Moon and R. T. Tranquillo, *Fibroblast-populated collagen microsphere assay of cell traction force: Part* 1*. Continuum model*, AIChE J., 39 (1993), pp. 163–177.

[17] J. D. Murray, *Mathematical Biology* II: *Spatial Models and Biomedical Applications*, Springer-Verlag, New York, 2003.

[18] J. D. Murray and P. K. Maini, *A new approach to the generation of pattern and form in embryology*, Sci. Prog., 70 (1986), pp. 539–553.

[19] J. D. Murray, P. K. Maini, and R. T. Tranquillo, *Mechanochemical models for generating biological pattern and form in development*, Phys. Rep., 171 (1988), pp. 59–84.

[20] J. D. Murray and G. F. Oster, *Generation of biological pattern and form*, Math. Med. Biol., 1 (1984), pp. 51–75.

[21] J. D. Murray, G. F. Oster, and A. K. Harris, *A mechanical model for mesenchymal morphogenesis*, J. Math. Biol., 17 (1983), pp. 125–129.

[22] B. N. Nagorcka, V. S. Manoranjan, and J. D. Murray, *Complex spatial patterns from tissue interactions—an illustrative model*, J. Theoret. Biol., 128 (1987), pp. 359–374.

[23] G. A. Ngwa and P. K. Maini, *Spatio-temporal patterns in a mechanical model for mesenchymal morphogenesis*, J. Math. Biol., 33 (1995), pp. 489–520.

[24] G. M. Odell, G. F. Oster, P. Alberch, and B. Burnside, *The mechanical basis of morphogenesis:* I*. Epithelial folding and invagination*, Dev. Biol., 85 (1981), pp. 446–462.

[25] G. F. Oster and J. D. Murray, *Pattern formation models and developmental constraints*, J. Exp. Zool., 251 (1989), pp. 186–202.

[26] G. F. Oster, J. D. Murray, and A. K. Harris, *Mechanical aspects of mesenchymal morphogenesis*, Development, 78 (1983), pp. 83–125.

[27] A. S. Perelson, P. K. Maini, J. D. Murray, J. M. Hyman, and G. F. Oster, *Nonlinear pattern selection in a mechanical model for morphogenesis*, J. Math. Biol., 24 (1986), pp. 525–541.
[28] L. F. Shampine and M. W. Reichelt, *The MATLAB ODE suite*, SIAM J. Sci. Comput., 18 (1997), pp. 1–22.
[29] L. J. Shaw and J. D. Murray, *Analysis of a model for complex skin patterns*, SIAM J. Appl. Math., 50 (1990), pp. 628–648.
[30] R. T. Tranquillo, M. A. Durrani, and A. G. Moon, *Tissue engineering science: Consequences of cell traction force*, Cytotechnology, 10 (1992), pp. 225–250.
[31] A. M. Turing, *The chemical basis of morphogenesis*, Phil. Trans. Roy. Soc., 13 (1952), pp. 37–72.
[32] L. Wolpert, *Positional information and the spatial pattern of cellular differentiation*, J. Theor. Biol., 25 (1969), pp. 1–47.